COBEM 2023 27TH INTERNATIONAL CONGRESS OF MECHANICAL ENGENEERING

ABCM Brazilian Society of Mechanical Sciences and Engineering
27th ABCM International Congress of Mechanical Engineering
December 04-08, 2023, Florianópolis-SC, Brazil

COB-2023-1831
A STUDY ON THE EFFECTS OF POST-DESIGN FIBER REINFORCEMENTS IN STRUCTURAL RESPONSE OF METALLIC TRUSSES

Bárbara Thaís Jacques Minosso
Mechanical Engineering Department, Federal University of Rio Grande do Sul
Rua Sarmento Leite, 425, Porto Alegre, RS. 90050-170, Brazil.
barbara.minosso@ufrgs.br

Rogério José Marczak
Mechanical Engineering Department, Federal University of Rio Grande do Sul
Rua Sarmento Leite, 425, Porto Alegre, RS. 90050-170, Brazil.
rato@mecanica.ufrgs.br

Abstract. *Carbon fiber-reinforced epoxy composites have numerous applications being commonly used in applications with high structural demand. These materials can be manufactured through several processes, in the case of cylindrical tubes, one of the common processes is filament winding (FW). Many reticulated structures are manufactured using metal beams with a circular cross-section, without provision for future expansions in the project. Aiming for the reusability of these structures and increasing their service life, FW can be used to form an outer layer of fiber reinforced (FR) composite on the individual bars of existing structures in order to strengthen the structures and increase their load-bearing capacity. With the reinforcements, the isotropic beams become layered beams, changing the calculations of these structures. Based on this information, the objective of this work is to evaluate the mechanical behavior of steel tubes reinforced through FW with Toray T700-12K-50C carbon fiber and UF3369 epoxy resin system from TCR Composites, compare their mechanical behavior with the original structure, and quantify the increase in load capacity. Analysis was carried out through finite element models of spatial truss structures using beam elements. Different angles of fiber orientation were tested. The results show that the largest gain occurs with the orientation* $[\pm 25°]$ *and the value of the frequencies does not have significant changes.*

Keywords: *composite tube, fiber reinforced material, truss, mechanical response, filament winding.*

1. INTRODUCTION

Metallic structures formed by thin-walled tubular three-dimensional gantry elements are often used in mechanical and civil construction. Examples of these structures can be cited: towers, bridges, roofs of bus terminals, airports, stadiums and distribution centers, and crane structures, among others. Thin-walled piping is used due to its architectural appearance, greater durability, and better performance to the exposure of dynamic actions (Santos, 2023).

Carbon fiber/epoxy composites materials have better mechanical properties compared to metallic materials, such as high specific strength, lightness, high corrosion and fatigue resistance, low thermal conductivity, and high energy absorption. These advantages are responsible for the significant increase in the use of these materials in various sectors, such as automotive, aerospace, naval, offshore and civil construction (Das et al., 2019; Huang et al., 2020). In general, cylindrical carbon fiber reinforced polymer (CFRP) structures have been used in trusses, platforms, pressure vessels, and reservoirs (Mian et al., 2013).

According to Wang et al. (2020), the hybrid metal/composite configuration comes to be a balance point between performance and cost of the structure. This is related to the combination of properties, for example, the plastic deformation of the metal can cause a progressive deformation of the FR composite more stable and the high rigidity of the composite can increase the curvature stiffness of the metal as well as increase the energy absorption of the hybrid structure.

Among the manufacturing processes that can be used to produce tubular cylindrical structures, the filament winding (FW) process stands out. In this process, continuous fiber filaments impregnated with resin are rolled along a rotating chuck, forming a composite layer on the surface. The main advantage of this method is the automation of the process, which enables high precision in the positioning of the fibers, optimization of properties, increased structural efficiency, mass production, and low cost with material and manufacturing (Das et al., 2019; Azeem et al., 2022).

This work aims to evaluate the behavior of existing metal structures exposed to deformations under increased load. Finite element analysis is used to obtain the results and compare the original structures with the reinforced structures in order to predict the viability of the process.

2. MECHANICAL PROPERTIES

The structure of FW cylinders is more complex than classic laminate, due to the formation of zones where the fibers intertwine, forming a winding pattern. Due to the difficulty of including these undulations in the composite design, the Classic Theory of Laminates has been used for the design and analysis of cylindrical structures of FW. (Hernández-Moreno et al., 2008, Mian et al., 2013).

In the case of an orthotropic material, the stress-strain relationships have the form (Jones, 1999):

$$\begin{bmatrix} \sigma_1 \\ \sigma_2 \\ \sigma_3 \\ \tau_{23} \\ \tau_{13} \\ \tau_{12} \end{bmatrix} = \begin{bmatrix} C_{11} & C_{12} & C_{13} & 0 & 0 & 0 \\ C_{12} & C_{22} & C_{23} & 0 & 0 & 0 \\ C_{13} & C_{23} & C_{33} & 0 & 0 & 0 \\ 0 & 0 & 0 & C_{44} & 0 & 0 \\ 0 & 0 & 0 & 0 & C_{55} & 0 \\ 0 & 0 & 0 & 0 & 0 & C_{66} \end{bmatrix} \begin{bmatrix} \varepsilon_1 \\ \varepsilon_2 \\ \varepsilon_3 \\ \gamma_{23} \\ \gamma_{13} \\ \gamma_{12} \end{bmatrix}, \tag{1}$$

Considering a curved surface shell element, it is assumed that each element of the mesh is a thin plate. Thus, the problem can reduced to a laminated plate subjected to axial forces in two directions.

The Classical Theory of Laminates considers thin laminates charged in the plane, with all stress components in the off-plane direction (3 direction) being zero, i.e., $\sigma_3 = \tau_{23} = \tau_{13} = 0$. Thus, orthotropic stress-strain relationships Eqs. (1) are reduced to

$$\begin{bmatrix} \sigma_1 \\ \sigma_2 \\ \tau_{12} \end{bmatrix} = \begin{bmatrix} Q_{11} & Q_{12} & 0 \\ Q_{12} & Q_{22} & 0 \\ 0 & 0 & Q_{66} \end{bmatrix} \begin{bmatrix} \varepsilon_1 \\ \varepsilon_2 \\ \gamma_{12} \end{bmatrix}, \tag{2}$$

or, inversely

$$\begin{bmatrix} \varepsilon_1 \\ \varepsilon_2 \\ \gamma_{12} \end{bmatrix} = \begin{bmatrix} S_{11} & S_{12} & 0 \\ S_{12} & S_{22} & 0 \\ 0 & 0 & S_{66} \end{bmatrix} \begin{bmatrix} \sigma_1 \\ \sigma_2 \\ \tau_{12} \end{bmatrix}, \tag{3}$$

where

$$Q_{11} = \frac{E_1}{1-\nu_{12}\nu_{21}}, Q_{22} = \frac{E_2}{1-\nu_{12}\nu_{21}}, Q_{12} = \frac{\nu_{21}E_1}{1-\nu_{12}\nu_{21}}, Q_{66} = G_{12}, \tag{4}$$

and

$$S_{11} = \frac{1}{E_1}, S_{12} = -\frac{\nu_{12}}{E_1}, S_{22} = \frac{1}{E_2}, S_{66} = \frac{1}{G_{12}}, \tag{5}$$

being E_1, E_2, G_{12} and ν_{12} the engineering constants of the material.

In a laminate it is common that the main axes of the blade do not coincide with the reference axes of the laminate. Therefore, to obtain the properties of the composite material, the unidirectional mechanical properties must be transformed through the transformation matrix given by

$$[T]=\begin{bmatrix} m^2 & n^2 & 2mn \\ n^2 & m^2 & -2mn \\ -mn & mn & m^2-n^2 \end{bmatrix}, \tag{6}$$

where $m=\cos\theta$ and $n=\sin\theta$, where θ is the measured angle between the x-axis and the 1-axis.

The global stiffness matrix, or transform, of the layer is obtained by the equation

$$[Q]_{xy}=[T][Q]_{12}[T]^{-1}, \tag{7}$$

where $[Q]_{12}$ is the local stiffness matrix of the layer.

In FW laminates, each layer is formed by two plies, $+\theta$ and $-\theta$, and is therefore balanced. With the winding pattern it is possible to divide the laminate into unit cells, which correspond to a single diamond-shape region, which can be divided into two parts separated by the undulation zone where roving cross over. Disregarding the undulation zone, the rhombus is divided into two triangles, one of laminate $\pm\theta$ and other $\mp\theta$. Because it is balanced, the stacking sequence does not interfere with the properties. Hernández-Moreno et al. (2008) proposed the use of the rule of mixtures to find the properties of a layer, considering that each ply corresponds to 50% of the volume of the layer,

$$[Q_{ij}]_{fw}=\sum_{k=1}^{2} V_k [Q_{ij}]_k, \tag{8}$$

where $[Q_{ij}]_{fw}$ is the stiffness matrix of a FW layer, V_k and $[Q_{ij}]_k$ is the volume and stiffness matrix of the unidirectional ply k, respectively.

The deformations at any point of the laminate can be found through the deformation in the middle plane and the curvatures of the laminate through the relation

$$\begin{bmatrix} \varepsilon_x \\ \varepsilon_y \\ \gamma_{xy} \end{bmatrix}=\begin{bmatrix} \varepsilon_x^0 \\ \varepsilon_y^0 \\ \gamma_{xy}^0 \end{bmatrix}+z\begin{bmatrix} \kappa_x \\ \kappa_y \\ \kappa_{xy} \end{bmatrix}, \tag{9}$$

where $\varepsilon_x^0, \varepsilon_y^0, \gamma_{xy}^0$ and $\kappa_x, \kappa_y, \kappa_{xy}$ are the deformations and curvatures in the middle plane, respectively, and z is a general point through the thickness of the laminate.

The resulting forces and moments are given as

$$\begin{bmatrix} N \\ M \end{bmatrix}=\begin{bmatrix} A & B \\ B & D \end{bmatrix}\begin{bmatrix} \varepsilon^0 \\ \kappa \end{bmatrix}, \tag{10}$$

where ε^0 and κ are the deformations and curvatures in the midline, N and M are the resulting forces and moments per unit length and A, B and D are the stiffness matrices of the laminate, with for uncoupled laminates, defined as

$$[A_{ij}]=\sum_{k=1}^{n}[Q_{ij}]^k (z_k-z_{k-1}), \tag{11}$$

$$[B_{ij}]=\frac{1}{2}\sum_{k=1}^{n}[Q_{ij}]^k \left(z_k^2-z_{k-1}^2\right), \tag{12}$$

$$[D_{ij}]=\frac{1}{3}\sum_{k=1}^{n}[Q_{ij}]^k \left(z_k^3-z_{k-1}^3\right), \tag{13}$$

where

A_{ij} extensional stiffness of the laminate;

B_{ij} bending-extension coupling stiffness;

D_{ij} flexural stiffness;

Q_{ij} overall stiffness layer; and

z_k position of the layer k relative to the reference plane, obtained from the stacking sequence, as illustrated in Figure 1.

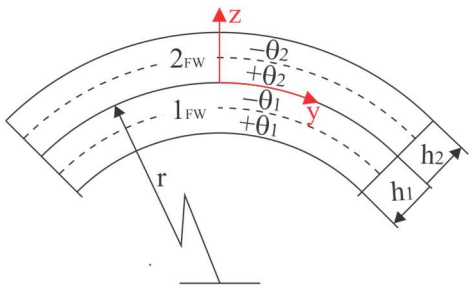

Figure 1. Stacking sequence and layer position.

From the stiffness matrices $[A]$, $[B]$, and $[D]$ it is possible to identify the engineering constants of the laminate in the plane state of stress with Eq. (14) and for the tension bending state with Eq. (15).

$$E_1 = \frac{1}{\left(A^{-1}\right)_{11} h}, E_2 = \frac{1}{\left(A^{-1}\right)_{22} h}, G_{12} = \frac{1}{\left(A^{-1}\right)_{66} h}, \nu_{12} = \frac{\left(A^{-1}\right)_{12}}{\left(A^{-1}\right)_{11}}, \nu_{21} = \frac{\left(A^{-1}\right)_{12}}{\left(A^{-1}\right)_{22}}, \tag{14}$$

$$E_1 = \frac{12}{\left(D^{-1}\right)_{11} h^3}, E_2 = \frac{12}{\left(D^{-1}\right)_{22} h^3}, G_{12} = \frac{12}{\left(D^{-1}\right)_{66} h^3}, \nu_{12} = \frac{\left(D^{-1}\right)_{12}}{\left(D^{-1}\right)_{11}}, \nu_{21} = \frac{\left(D^{-1}\right)_{12}}{\left(D^{-1}\right)_{22}}, \tag{15}$$

With these constants it is possible to present a laminate material in the form homogeneous material, and the properties of the material are defined by these constants (Smolnicki e Stabla, 2019).

3. FINITE ELEMENT ANALYSIS

Beam elements are widely used in structural engineering to model lattice structures. According to Bathe (2014), the most effective way to evaluate the stiffness matrices of these elements is through the use of the principle of virtual work, which is the basic relationship used for the formulation of elements by the displacement method.

Throughout this work, we used the Timoshenko beam element to model the one-dimensional beam segments of the structures analyzed. The main difference to the conventional Euler-Bernoulli element is in the consideration of the transverse shear deformation, which can be significant in short beams composing complex reticulated structures. The other main difference relies in the use of quadratic shape functions to interpolate displacement and rotations, whereas the Bernoulli element uses cubic Hemite polynomials. Therefore, special care was taken to ensure that the mesh was sufficient for good convergence. We used five elements per meter as a general rule, therefore compensating for any deficiency in the global shape function for the displacement response.

The remaining of the formulation remains the same of usual Galerkin's method, that is, no substitute strain field was used, leading to the final system

$$[K]\{d\} = \{F\}, \tag{16}$$

where $[K]$ is the stiffness matrix, $\{d\}$ is the displacement vector, and $\{F\}$ is the force vector.

In the present implementation, existing structures in structural steel, with their original dimensions and thicknesses were numerically modeled in ANSYS® software using the BEAM189 elements, which correspond to the aforementioned Timoshenko element (Ansys, 2021). For the reinforcement, a new beam structure was modeled, having as the internal diameter of the tubes the dimension of the outer diameter of the steel tubes. The thickness of the composite material considered is 1 mm, corresponding to two layers of FW. It was considered perfect connection in steel and composite. The

3 previously selected settings were used to identify the best configuration for each case. The structures were loaded with the original loads in order to identify the resistance gain with the reinforcement. The first vibration modes and their respective frequencies were also evaluated.

4. NATURAL FREQUENCIES

The system of equations constituting the equations of motion for an undamped system can be written as

$$[M]\{\ddot{u}\} + [K]\{u\} = \{F\}, \tag{17}$$

where $[M]$ and $[K]$ are the matrices of mass and stiffness, respectively and $\{u\}$, $\{\ddot{u}\}$ and $\{F\}$ are the vectors of displacement, acceleration, and force, respectively.

The problem of free vibrations requires $\{F\} = 0$ and has as its solution

$$\{u\} = \{a\}\sin(\omega t - \alpha), \tag{18}$$

where $\{a\}$ is the amplitude of motion vector, ω is the natural frequency, t is the time, and α is the angular acceleration.

Making the substitutions and rearranging the terms

$$\left[[K] - \omega^2[M]\right]\{a\} = \{0\}, \tag{19}$$

The nontrivial solution of Eq. (19), for which not all $a_i = 0$, requires that the determinant of the matrix factor $\{a\}$ be equal to zero, therefore

$$\left[[K] - \omega^2[M]\right] = 0. \tag{20}$$

The expansion of the determinant of Eq. (20) results in a polynomial equation of degree n in ω^2, this equation is known as the characteristic equation of the system. The roots of this equation provide the natural frequencies ω_i, for $i = 1,2,\dots,n$, being n the modes of vibration (Paz, 2019).

The natural frequency of a system refers to the frequency of the first mode of the structure without applied loads and can be obtained through the elementary equation:

$$f = \frac{\omega}{2\pi}, \tag{21}$$

where f is the natural frequency, in Hz, and ω is called the circular or angular natural frequency, measured in (rad/s) (Paz, 2019).

5. MATERIAL PROPERTIES

The metal structures under study are made of structural steel. For the numerical analysis, the mechanical properties of the steel given by NBR 8800/08 were considered. This standard establishes the basic requirements that must be obeyed in the design at ambient temperature of steel structures. Table 1 presents the mechanical properties of structural steel (ABNT, 2008).

Table 1. Mechanical properties of structural steel (ABNT, 2008).

Properties	Symbol	Value
Elastic modulus	E_a (GPa)	200
Transversal elastic modulus	G (GPa)	77
Poisson's ratio	ν_a	0.3
Yield stress	σ_{esc} (MPa)	250
Ultimate tensile stress	σ_{rup} (MPa)	400
Density	ρ (kg/m³)	7850

For the reinforcement, the pre-impregnated fiber (towpreg) of Toray T700-12K-50C carbon fiber and UF3369 epoxy resin from the manufacturer TCR Composites was chosen as composite material. The excellent stress-strain ratio of the carbon fiber was taken into account. For the present study, the lamina properties of this material were used (Table 2), with a volumetric fiber content ≈ 72% obtained by Almeida et al. (2016).

Table 2. Mechanical properties of composite (Almeida et al., 2016).

Properties	Symbol	Value
Longitudinal elastic modulus	E_1 (GPa)	129.3
Transversal elastic modulus	E_2 (GPa)	9.11
Poisson's ratio in plane 1-2	$\nu_{12} = \nu_{13}$	0.32
Poisson's ratio in plane 2-3	ν_{23}	0.35
In-plane shear modulus	$G_{12} = G_{13}$ (GPa)	5.44
Transverse shear modulus in plane 2-3	G_{23} (GPa)	2.10
Longitudinal tensile strength	X_t (MPa)	1409.9
Transversal tensile strength	Y_t (MPa)	42.5
Longitudinal compressive strength	X_c (MPa)	-740.0
Transversal compressive strength	Y_c (MPa)	-140.3
In-plane shear strength	S_{12} (MPa)	68.9
Density(1)	ρ (kg/m³)	1626

(1)Calculated from the rule of mixtures.

The properties of the carbon fiber/epoxy composite material were obtained with the aid of script in MATLAB following the equations of the previous topic. The thickness of each FW layer considered was $t_l \approx 0.5$ mm, and each layer corresponds to 2 plies, $+\theta$ and $-\theta$. The objective was to identify the best angles for numerical analysis. The graph in Figure 2 shows the elastic constants according to the angle of orientation of the fibers for a total of 2 layers of FW. The modulus of stiffness, bending, traction and torsion are shown in Figure 3, for a tube with an internal diameter of 33.4 mm.

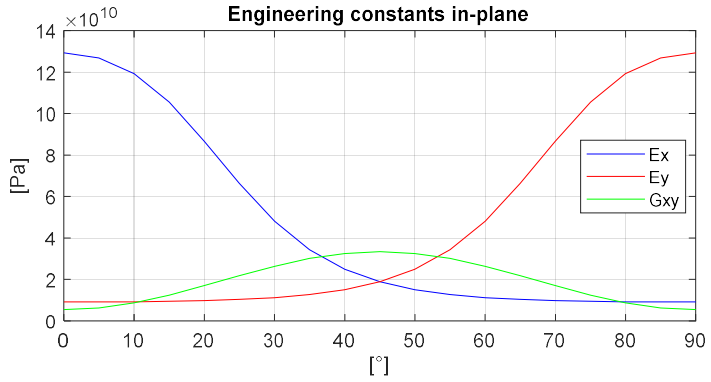

Figure 2. Composite material properties vs orientation angle.

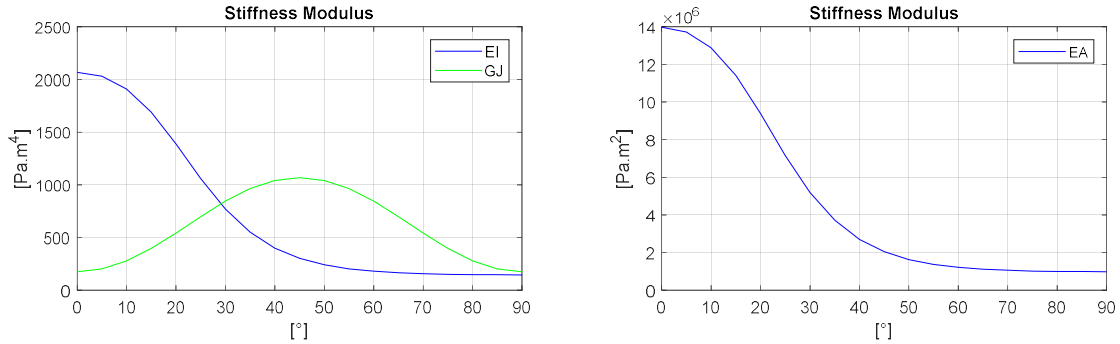

Figure 3. Stiffness modulus vs orientation angle: a) bending and torsion, (b) tension.

Based on the graphs in Figure 3, 3 different configurations were selected for the next step: $[\pm 25°]_2$, $[\pm 30°]_2$ and $[\pm 45°]_2$. The ideal orientation for traction and bending is 0°, while for torsion it is 45°, however, due to the limitations of the manufacturing process the angle of 25° was adopted instead of 0°.

The mechanical properties of the composite with these winding configurations are presented in Table 3.

Table 3. Mechanical properties used in the simulations.

Properties	Value		
	$[\pm 25°]_2$	$[\pm 30°]_2$	$[\pm 45°]_2$
E_x (GPa)	66.254	48.120	18.926
$E_y = E_z$ (GPa)	10.345	11.256	18.926
ν_{xy}	1.3428	1.2929	0.7395
$\nu_{yz} = \nu_{xz}$	0.35	0.35	0.35
$G_{xy} = G_{yz} = G_{xz}$ (GPa)	21.839	26.399	33.386

6. RESULTS AND DISCUSSIONS

The first case analyzed is the result of layout optimization performed by Santos (2023). It is a cantilever truss structure with a concentrated load applied at end B. Two load conditions are tested: 1) $F_1 = 120$ kN e $F_2 = 0$, and 2) $F_1 = 0$ e $F_2 = 60$ kN. The geometry of the structure and load conditions are shown in Figure 4. The mass of the structure in steel is 4431 kg, the mass of the reinforcing material, 122 kg, resulting in a total mass of 4553 kg.

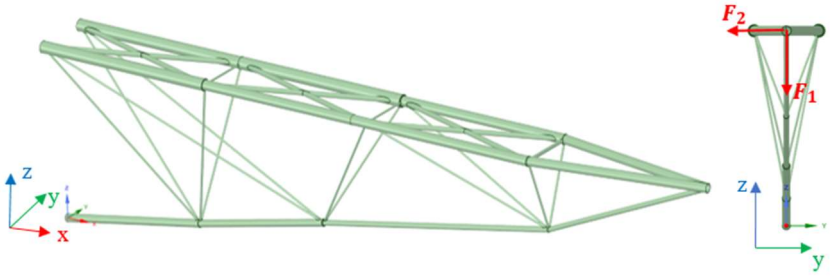

Figure 4. Cantilever structure optimized by Santos (2023).

For both loads, the displacements obtained are shown in Table 4, where it is possible to identify that the Steel+$[\pm 25°]_2$ configuration presents better performance, having the lowest displacement, with a reduction of approximately 4% in relation to the original structure.

Table 4. Resulting displacements for the different loading conditions.

Configuration	Displacement (mm)			
	Condition 1	Reduction %	Condition 2	Reduction %
Steel	45.756	-	82.461	-
Steel+$[\pm 25°]_2$	43.833	4.20	78.521	4.78
Steel+$[\pm 30°]_2$	44.344	3.08	79.406	3.70
Steel+$[\pm 45°]_2$	45.19	1.24	80.872	1.93

The frequencies for the first four vibration modes are presented in Table 5. Through them it is possible to evaluate the frequency variation of each mode according to the angular orientation of the reinforcement. It can be verified that the Steel+$[\pm 45°]_2$ configuration presents the worst results, reducing the value of the natural frequency of the structure, while the Steel+$[\pm 25°]_2$ configuration is the one that presents the best performance, since it increased the natural frequency by at least 0.8%.

Table 5. Vibration mode of cantilever beam.

Vibration Mode	Frequencies (Hz)			
	Steel	Steel+$[\pm 25°]_2$	Steel+$[\pm 30°]_2$	Steel+$[\pm 45°]_2$
Mode I	4.7713	4.8146	4.786	4.7393
Mode II	8.6911	8.8278	8.7603	8.6486
Mode III	10.137	10.376	10.281	10.127

Aiming the reduction of the displacement of the structure by 10% and taking into account that the thickness of the steel is 8 mm and 1 mm of composite may not be enough for a significant gain in stiffness, a new analysis was carried

out, increasing the number of FW layers of the reinforcement. The $[\pm 25°]$ configuration was used, since it showed better performance among the three configurations under study. The maximum desired displacements are 40.484 mm for condition 1 and 71.09 mm for condition 2. For both cases of loading, this condition was met using 3 FW layers, whose final thickness is equivalent to 1.5 mm. Evaluating the natural frequencies of the structure, an increase of 2.73% compared to the original structure is perceived.

The second case of this study is a footbridge with a span of approximately 30m. Originally optimized in the study by Ghasemi et al. (2023), the structure was considered with the dimensions of tubular sections obtained by the BGP method, which presented lower total weight. The objective is to analyze the possibility of deploying the structure in a place where it is not possible to install the central support base. Once considered as a bi-supported beam, the footbridge was simulated numerically in order to identify its behavior in the face of deflection and the vibration modes of the structure. Afterwards, the structure went through the reinforcements following the same way as the previous case, evaluating its behavior before the reinforcement of the steel with carbon fiber/epoxy.

The structure with the representation of the boundary conditions is presented in Figure 5. The structure is loaded with wind loads laterally, being 1.5 kN at deck and 0.34 kN at base, and with the moving load generated by pedestrians. According to the standards, the mobile load considered for bridges due to the transit of people should be 5 kN/m² distributed in the pipes that support the floor. The mass of the structure in steel is 6048.6 kg, the mass of the reinforcing material, 391.12 kg, resulting in a total mass of 6439.8 kg.

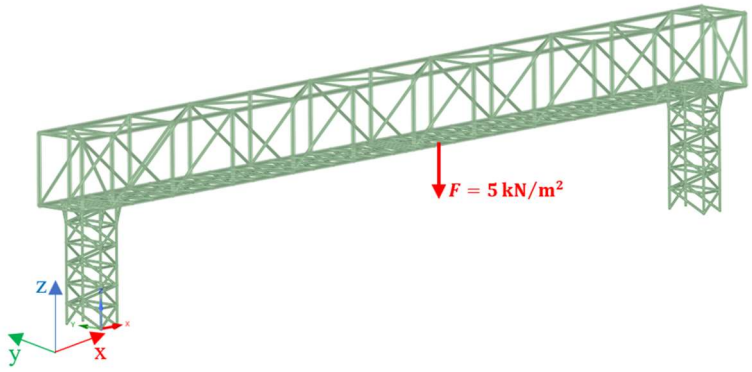

Figure 5. Footbridge structure adapted of Ghasemi et al. (2023).

Table 6 shows the resulting displacements caused by the applied load. It can be seen that the Steel+$[\pm 25°]_2$ configuration is the one that presented the best performance, with a reduction of 34.48% in the displacement compared to the steel structure. However, comparing the different angles of orientation of the reinforcement, there was no significant difference.

Table 6. Resulting displacements for the structure without central base.

Configuration	Displacement (mm)	Reduction %
Steel	16.906	-
Steel+$[\pm 25°]_2$	11.071	34.46
Steel+$[\pm 30°]_2$	11.329	32.93
Steel+$[\pm 45°]_2$	11.772	30.31

The vibration modes of the structure and their respective frequencies were obtained through modal analysis and are presented in Table 7. It can be concluded that as in the structure previously analyzed, the Steel+$[\pm 25°]_2$ configuration showed better performance, increasing the natural frequency of the structure, whereas the Steel+$[\pm 45°]_2$ configuration caused the reduction of the values of the natural frequencies of the structure, this is related to fact that there was both the change in stiffness and in the mass of the structure, because there was no significant increase in stiffness for these reinforcement orientations, there was a reduction in the natural frequency.

Table 7. Vibration mode of structure.

Vibration Mode	Frequencies (Hz)			
	Steel	Steel+$[\pm 25°]_2$	Steel+$[\pm 30°]_2$	Steel+$[\pm 45°]_2$
Mode I	6.9089	7.002	6.923	6.792
Mode II	20.392	20.727	20.475	20.062

7. CONCLUSION

This study allowed to identify the stiffness gain when the metal structure is reinforced by CFRP. For cases under traction and bending, the lower the winding angle of the FW fibers, the greater the longitudinal elasticity modulus and, consecutively, the stiffness modulus, which is proven through the analytical analysis of the mechanical properties of the CFRP and by comparing the behavior of the structure against different angles of orientation of the reinforcement.

Comparing the results of the different structures, it is clear that the load gain for the same FW configurations is directly related to the original configurations of the steel structure. The first case presented a steel thickness of 8 mm, presenting a small reduction of displacements with the standardized load, which indicates that the thickness of 1 mm referring to 2 FW layers is not sufficient for a significant gain. On the other hand, the second case, whose maximum thickness is 4 mm, 2 FW layers are enough to raise the rigidity of the structure, providing a considerable load gain.

As for the vibration frequencies, the results show little variation in values, being directly related to the mass gain of the structure, which counter-balances the stiffness gain.

8. ACKNOWLEDGEMENTS

We thank the CAPES for the financial support to present this paper. The second author acknowledges CNPq grant 317140/2021-3.

9. REFERENCES

Almeida Jr., J.H.S., Souza, S.D.B., Botelho, E.C., Amico, S.C., 2016, Carbon fiber-reinforced epoxy filament-wound composite laminates exposed to hygrothermal conditioning, Journal of Materials Science, Vol. 51, pp. 4697-4708.

Ansys, Inc., 2021, Useful Solutions for Standard Problems.

Associação Brasileira de Normas Técnicas, ABNT, 2008, NBR 8800/08: Projeto de estruturas de aço e de estruturas mistas de aço e concreto de edifícios, 237p.

Azeem, M., Ya, H.H., Alam, M.A., Kumar, M., Stabla, P., Smolnicki, M., Gemi, L., Khan, R., Ahmed, T., Ma, Q., Sadique, M.R., Mojhtar, A.A., Mustapha, M., 2022, Application of filament winding technology in composite pressure vessels and challenges: a review, Journal of Energy Storage, Vol. 49, pp. 103468.

Bathe, K.J., 2014, *Finite Element Procedures*, 2nd ed, Klaus-Jurgen Bathe.

Das, T.K., Ghosh, P., and Das, N.C., 2019, Preparation, development, outcomes, and application versatility of carbon fiber-based polymer composites: a review, Advanced Composites and Hybrid Materials, Vol. 2, pp. 214-233.

Ghasemi, M.R., Salarnia, A., Ghasri, M., 2023, Optimal design of steel structures using innovative black widow algorithm hybridized with greedy sensitivity-based particle swarm optimization technique, Journal of Soft Computing in Civil Engineering, pp. 55-84.

Hernández-Moreno, H., Douchin, B., Collombet, F., Choqueuse, D., Davies, P., 2008, Influence of winding pattern on the mechanical behavior of filament wound composite cylinders under external pressure, Composite Science and Technology, Vol. 68, pp. 1015-1024.

Huang, Z., Qian, X., Su, Z., Pham, D., Sridhar, N., 2020, Experimental investigation and damage simulation of large-scaled filament wound composite pipes, Composites Part B: Engineering, Vol. 184, pp. 107639.

Hughes, T.J.R., 1987, *The Finite Element Method: Linear Static and Dynamic Finite Element Analysis*, 1st ed, Prentice-Hall, Inc.

Jones, R.M., 1999, *Mechanics of composite materials*, 2nd ed, Taylor & Francis.

Mian, H.H., Wang, G., Dar, U.A., Zhang, W., 2013, Optimization of composite material system and lay-up to achieve minimum weight pressure vessel, Applied Composite Materials, Vol. 20, pp. 873-889.

Paz, M.P., Kim, Y.H., 2019, *Structural Dynamics*, 6th ed., Springer.

Santos, P.S., 2023. *Layout and topology optimization of three-dimensional tubular gantries with semi-rigid connections including mixed variables and reduction of complexity (in Portuguese)*. Master's thesis, Graduate Program in Mechanical Engineering, State University of Santa Catarina, Joinville, Brasil.

Smolnick, M., Stabla, P., 2019, Finite element method analysis of fibre-metal laminates considering different approaches to material model, SN Applied Sciences, Vol. 1, pp. 467.

Wang, Z., Jin, X., Çi, Q., Sun, G., 2020, On crashworthiness design of hybrid metal-composite structures, International Journal of Mechanical Sciences, Vol. 171, pp. 105380.

10. RESPONSIBILITY NOTICE

The authors are the only responsible for the printed material included in this paper.